Journal of Nuclear Materials 607 (2025) 155673

Contents lists available at ScienceDirect

Journal of Nuclear Materials

journal homepage: www.elsevier.com/locate/jnucmat

Effect of irradiation parameters on defect evolution in neutron irradiated tungsten

M. Klimenkov [a,*], U. Jäntsch [a], M. Rieth [a], H.C. Schneider [b], D. Terentyev [c], W. Van Renterghem [c]

[a] Karlsruhe Institute of Technology (KIT), Institute for Applied Materials - Applied Materials Physics, Karlsruhe 76021, Germany
[b] Karlsruhe Institute of Technology (KIT), Institute for Applied Materials - Mechanics of Materials and Interfaces, Karlsruhe 76021, Germany
[c] SCK CEN, Nuclear Energy Technology Institute, Boeretang 200, Mol 2400, Belgium

HIGHLIGHTS

- Determination of the effect of the irradiation parameters on the size and number density of the defects.
- Comprehensive study of Re- and Os-segregation on voids and dislocation loops. Evidence of segregation on defects at the lowest damage dose of 0.1 dpa.
- Determination of the effect of the line dislocations and grain boundaries on defects formation.

GRAPHICAL ABSTRACT

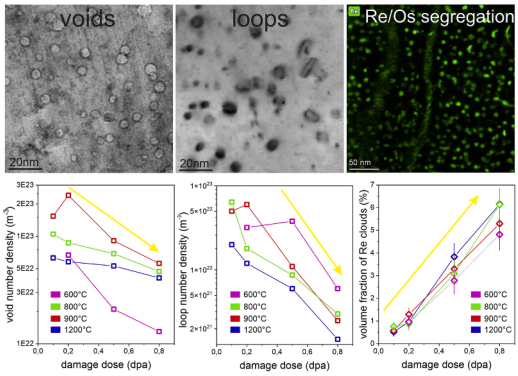

ARTICLE INFO

Keywords:
Tungsten
Neutron irradiation
Microstructure
Transmutation
Voids
Radiation induced defects

ABSTRACT

The article presents a microstructural examination of neutron-irradiated tungsten (W), that was irradiated to four damage doses of 0.1 dpa, 0.2 dpa, 0.5 dpa and 0.8 dpa and at four temperatures of 600°C, 800°C, 900°C and 1200°C in the BR2 material test reactor (Mol, Belgium). The irradiation parameters cover a wide range that enables a comprehensive study of defect formation and evolution. The experimental work includes imaging and quantitative analysis of radiation induced voids and dislocation loops as well as the visualization of the distribution of the transmutation induced Re and Os. It demonstrates the dose- and temperature-dependent evolution of defect's size and number density as well as the segregation behavior of Re and Os at these defects. It was proven that the size of the defects increases, while their number density decreases with increasing damage dose. The formation of nanometer-sized Re–Os precipitates with elongated shape was detected in samples irradiated at 0.8 dpa. The large-scale EDX analysis showed the influence of grain and sub-grain boundaries as well as line dislocations on defect formation and thus on Re and Os-segregation behavior.

* Corresponding author.
E-mail address: michael.klimenkov@kit.edu (M. Klimenkov).

https://doi.org/10.1016/j.jnucmat.2025.155673
Received 10 July 2024; Received in revised form 27 January 2025; Accepted 2 February 2025
Available online 3 February 2025

1. Introduction

The development and construction of fusion reactors such as ITER or DEMO in recent years requires the development of new structural materials that can withstand the new challenging requirements. Tungsten (W) and W-based alloys are the most important materials for plasma facing components, mainly because of the high sputtering threshold, high thermal conductivity and resistance, and low tritium retention [1–3]. Knowledge of W radiation resistance will provide valuable information about the stability of the components that are exposed to the high-energy plasma and high temperature during the fusion process. The effects of such exposures are enhanced neutron-induced embrittlement, which limits the long-term operation of W components. Neutron embrittlement in pure tungsten, which suffers a damage of –2–6 dpa per full power year in the plasma-facing components, occurs up to irradiation temperatures of at least 600–800°C [4–6]. The irradiation at higher temperatures, on the other hand, leads to recrystallization and related material softening, hereby increasing the thermal fatigue of W [7]. In order to determine the operational limits of W components, wide-ranging investigations are required to show the behavior of W under neutron irradiation.

Experimental data on the microstructure of neutron irradiated W, available in the scientific literature, are summarized in ref. [8]. Despite extensive experimental work, the microstructural understanding of defect formation and evolution is still rather incomplete. The reason for this can be found in the different irradiation conditions and the sensitivity of the final results to minor factors. Consequently, the results of different irradiation campaigns are only partially comparable. This is because the transmutation rates of Re and Os are different for the various reactor types, which finally leads to the different their contents [9–11]. It is known that the presence of Re and Os affects the formation of defects and thus the mechanical properties of W [10,12]. Other, less important factors, such as the position of the sample in the reactor, the shielding, the precise control of the temperature during irradiation, the duration of the reactor cycles and others, can also influence the defect formation in W.

It is therefore essential to study the effect of neutron irradiation in W irradiated under similar conditions in order to observe the defects evolution as a function of damage or temperature. For this propose, tungsten was irradiated to four damage doses of 0.1 dpa, 0.2 dpa, 0.5 dpa and 0.8 dpa and four temperatures 600°C, 800°C, 900°C and 1200°C in the BR2 material test reactor (Mol, Belgium). The experimental matrix allows conclusions concerning the influence of the irradiation conditions (damage dose and irradiation temperature) on defect formation. Additionally, the segregation behavior of Re and Os on voids and dislocation loops was studied. High resolution TEM analysis demonstrates the formation of elongated nanometer-sized precipitates in W irradiated to 0.8 dpa. Microstructure analysis not only allows prediction of the service life of W components but also experimental validation of the theoretical modelling of radiation-induced defects in W.

2. Experimental

The investigated polycrystalline W with a purity of 99.97 wt.% was provided by PLANSEE SE, Austria as a plate of 1 mm thickness. The plate was produced by cold rolling and processed without additional stress-relieving treatment. The material was neutron irradiated to the damage doses of 0.1 dpa, 0.2 dpa, 0.5 dpa and 0.8 dpa (targeted values) at 600°C, 800°C, 900°C and 1200°C irradiation temperatures in the Belgian Nuclear Research Center SCK CEN, Mol (Belgium). In this study, 15 samples from a total of 16 irradiated samples were analyzed using TEM. Only one irradiation condition, 0.1 dpa/600°C, was not available for this study.

The irradiation was performed directly inside a channel within a fuel element. The irradiation rig was made of a tick-wall pressurized tube, which had a dual function: pressure-barrier and shielding to screen thermal neutrons. The irradiation was performed in Helium to prevent oxidation under high temperature irradiation exposure. The total irradiation time was 28–186 days (depending on the specific capsule) and the neutron flux was $(1.5–2.6) \times 10^{14}$ (E > 0.1 MeV), $(0.6–1.2) \times 10^{14}$ (E > 1 MeV) n/cm^2/s. The neutron flux was calculated using the MCNPX 2.7.0 code as well as confirmed by dosimetry measurements using Fe and Nb dosimeters, applied to measure the fast neutron fluence (>1 MeV) [13]. The dpa cross sections for W have been prepared from the JENDL4 file (MT444) for a threshold displacement energy of 55 eV. The concentration of the transmutation induced Re and Os and the damage doses calculated after carrying out the experiment are given in Table 1.

The irradiation temperature has been checked by means of passive sensors such as SiC. The mean irradiation temperature is defined by the design (i.e. sample dimension, position of the capsule in the reactor, information on the neutron and gamma fluxes) and the typical variation of the temperature during the irradiation is about ± (5–10)%

Since the material is radioactive, it was advantageous to use focused ion beam milling (FIB) for sample preparation in order to limit the activity of the TEM samples, which interferes with the chemical analysis. The thin lamellae were prepared in a Scios FIB/SEM instrument (product of Thermo Fisher Scientific Inc.) and attached to a molybdenum grid. After FIB preparation the lamellae were flash polished in 1 % NaOH water solution using the method described in ref. [14] to remove defects introduced during ion beam milling. This step enables the analysis of voids and dislocation loops, which are poorly visible due to the surface damage caused by the FIB.

The microstructural examination was carried out using a Talos F200X transmission electron microscope (TEM) (product of Thermo Fisher Scientific Inc.) equipped with four energy-dispersive X-ray (EDX) detectors. The EDX detector resolution is specified by the manufacturer as ≤136 eV at Mn-Kα. At the W-Lα (E = 8.396 keV) the energy resolution has a value of about 150–160 eV, which is sufficient to separate the W-Lα, Re-Lα and Os-Lα X-ray lines. The TEM images and selected area diffraction pattern (SAED) were acquired by using a Ceta 16 M CCD camera. The STEM-EDX maps were acquired in the Velox software using 512×512 pixels and a spectral dispersion of 5 eV. ImageJ software was used for statistical analysis of the TEM images [15].

Voids were visualized using under-focused bright field (BF) imaging, displaying them with bright contrast compared to the matrix. The images of loops were taken using diffraction contrast in the dark field (DF) imaging applying scanning TEM (STEM) [16]. The DF images are displayed with inverted intensity contrast, which allows for a better visualization of low intensity defects. The thickness of the sample that was used for number density calculations was measured using low loss electron energy loss spectroscopy (EELS). Due to the considerable local variations of thickness caused by the flash polishing procedure, the average thickness of the examined area was taken for the calculation of the defect number density.

3. Results

3.1. Dose- and temperature-dependent defect formation

The micrographs in Fig. 1 show the microstructure of W irradiated at 600°C-0.1 dpa (a), 1200°C-0.1 dpa (b) and 1200°C-0.8 dpa (c). The grain structure of 600°C-0.1 dpa irradiated W is not changed by the irradiation and can be regarded as original, “as-delivered” structure. Its microstructure consists of the elongated grains with 1–3 μm length and up to 1 μm width. The average thickness of the grains is –600 nm The

Table 1
Content of transmutation induced elements for different damage doses.

damage dose (dpa)	0.12	0.18	0.51	0.75
Re (FISPACT) (at. %)	0.41	0.59	1.60	2.1
Os (FISPACT) (at. %)	0.007	0.014	0.13	0.22

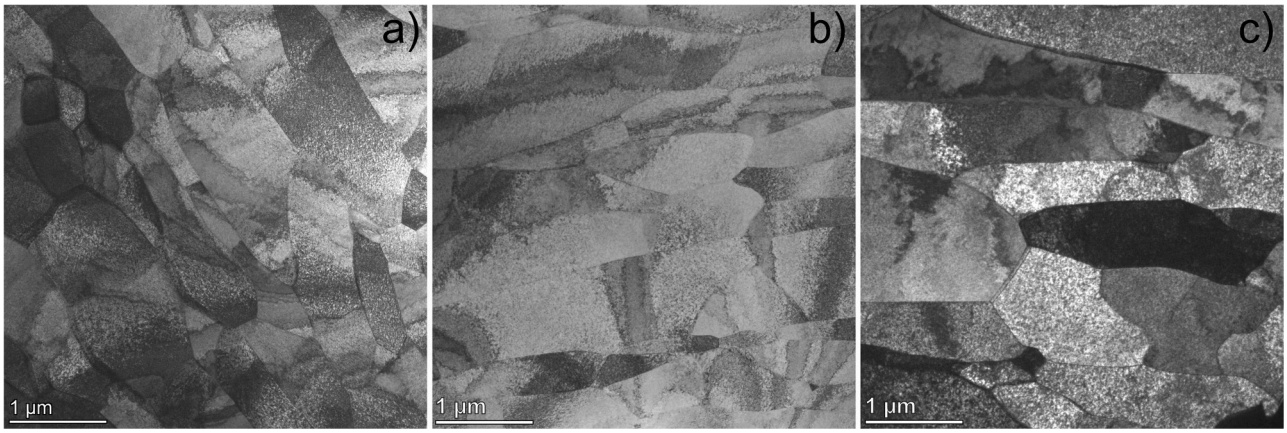

Fig. 1. TEM images of the grain structure of W irradiated at 600°C with 0.2 dpa (a), 1200°C with 0.1 dpa (b), and 1200°C with 0.8 dpa (c).

width of the grains in W, which was irradiated at 1200°C-0.1 dpa and 1200°C-0.8 dpa, is about 10 and 25 % larger than as delivered (Fig. 1b, c). The sample irradiated at 1200°C-0.8 dpa exhibits a higher proportion of sub-grains - the grains with minimal (<1°) misorientation to neighboring grains, separated by a dislocation network [9]. Due to the large variations in grain length, it is not possible to draw conclusions concerning radiation-induced recrystallization. The density of the line dislocations is estimated to be in the range of ~10^{12} m^{-2} for all irradiation states, which indicates a recovery of the microstructure after cold rolling during irradiation at elevated temperature.

The formation of voids and dislocation loops were observed at all radiation conditions. Fig. 2 illustrates the voids in under-focused BF images and Fig. 3 shows the loops formed in W in inverted intensity DF images. The material irradiated at 600°C to 0.1 dpa was not available for TEM analysis, so the positions for these images remain empty in both Figures. The voids are uniformly distributed within the grains, but form a narrow, depleted zone around the grain boundaries, which will be considered later in this work. The dislocation loops, on the other hand, are less homogeneously distributed forming areas with a clearly higher or lower number density. At low damage doses (e.g., 0.1 dpa and 0.2 dpa) the majority of the loops is less than 5 nm in size. In the inverted intensity DF-TEM images they are visible as 'black dots'. At higher damage doses, the size of the loops increases, and they appear in the typical "coffee-bean" contrast. At 0.8 dpa, the formation of nanoscale precipitates also sets on. The loop statistics in these samples can be influenced by this factor, as the precipitates induce a similar contrast in TEM images as the loops.

The dose-dependent evolution of the defect's parameters is shown in Fig. 4 and numerical data can be found in Table 2. The void size tends to increase with the damage dose and with higher irradiation temperatures (a). The largest voids with an average size of 4.5 nm were found in the material irradiated at 1200°C to 0.8 dpa. At the lower temperatures the void size varied in the range between 1.8 and 3.5 nm. However, the void number density decreases by a factor of ~2.5 with increasing damage dose (b). Void swelling increases with the damage dose at 900°C and 1200°C, whereas it remains constant within the error range at 600°C and 800°C (c). The swelling values were measured as low as 0.25 %. The volume fraction of Re clouds reaches 5–6 % at 0.8 dpa damage (f).

The loop sizes and number densities are plotted in Fig. 4d,e. At low damage doses, the loops are visible as black dots with a size smaller than 5 nm. As the damage dose increases, the loop size increases and their number density decreases. At 0.8 dpa, their number is reduced by more than one order of magnitude compared to number density measured at 0.1 dpa damage dose.

3.2. Distribution transmutation induced Os and Re

The distribution of transmutation induced Re and Os is shown in Fig. 5 (600°C and 800°C) and Fig. 6 (900°C and 1200°C). The average Re and Os content in the sample is around 1-2 %, but these elements form enriched regions with concentrations of 5-15 %, spanning several nanometers in thickness, around voids and loops [17,18]. Since these regions do not show any distortion of the crystalline structure of W, they are referred to as "clouds" and not as "precipitates". The segregation of Re on radiation induced defects is detectable at all damage doses, whereas Os on the defects could only be detected at 0.5 dpa and 0.8 dpa. The formation of Os-rich precipitates with an elongated shape, which are presumably nanoscale precipitates or their precursors, was only detected at 0.8 dpa damage. At 600 and 800°C, even at the highest damage dose of 0.8 dpa, no clear evidence was found of Os rich precipitates. Os and Re show increased concentration around voids or loops, with no noticeable evidence of precipitates formation (Figure $5d_1$, d_1').

Segregation at the structural defects such as line dislocations and grain boundaries was also observed for all damaged doses and irradiation temperatures. For example, Re segregation on a line dislocation is well visible in Figure $5a_2$ or Figure $6c_2$.

Detailed analysis of the clouds with an elongated shape formed at 900 and 1200°C and 0.8 dpa damage show that they have a defined crystalline structure, which differs from the W structure. Three examples of such precipitates with a length up to 6 nm are show in Fig. 7. The precipitates could be located on the voids (a), or at a random location (b and c). The spots in the corresponding Fourier transform image attributed to the particles are marked by arrows. Their atomic distances were measured as 0.274 nm (a), 0.236 nm (b) and 0.425 nm (c) that could correspond to the d_{222}=0.276 nm, d_{004}=0.240 nm and to d_{012}=0.429 nm atomic planes of χ-$W(Re,Os)_3$ phase. The χ-$W(Re,Os)_3$ phase has a cubic structure with a=0.96 nm.

Nevertheless, these and other HRTEM results are not sufficient to clearly identify the crystal structure of the precipitates. The small precipitates in the HRTEM images show only one resolved atomic plane or, as they overlap with the matrix, show several spots in the Fourier transform that can be attributed to the overlap of the two structures. The available experimental data are not sufficient to conclude whether the σ-$W(Re,Os)_2$ or χ-$W(Re,Os)_3$ phase is formed. It is quite conceivable that these small particles, which size is in the range of a few lattice constants, have a structure that differs from the known phases.

The last column in Table 2 shows the number density of the nanoscale Re-rich clouds that have formed around the defects. In general, these values are very similar to the number densities of the voids formed at the same conditions. At the low damage doses, the number density of voids is higher than that of Re rich clouds because the Re signal was too

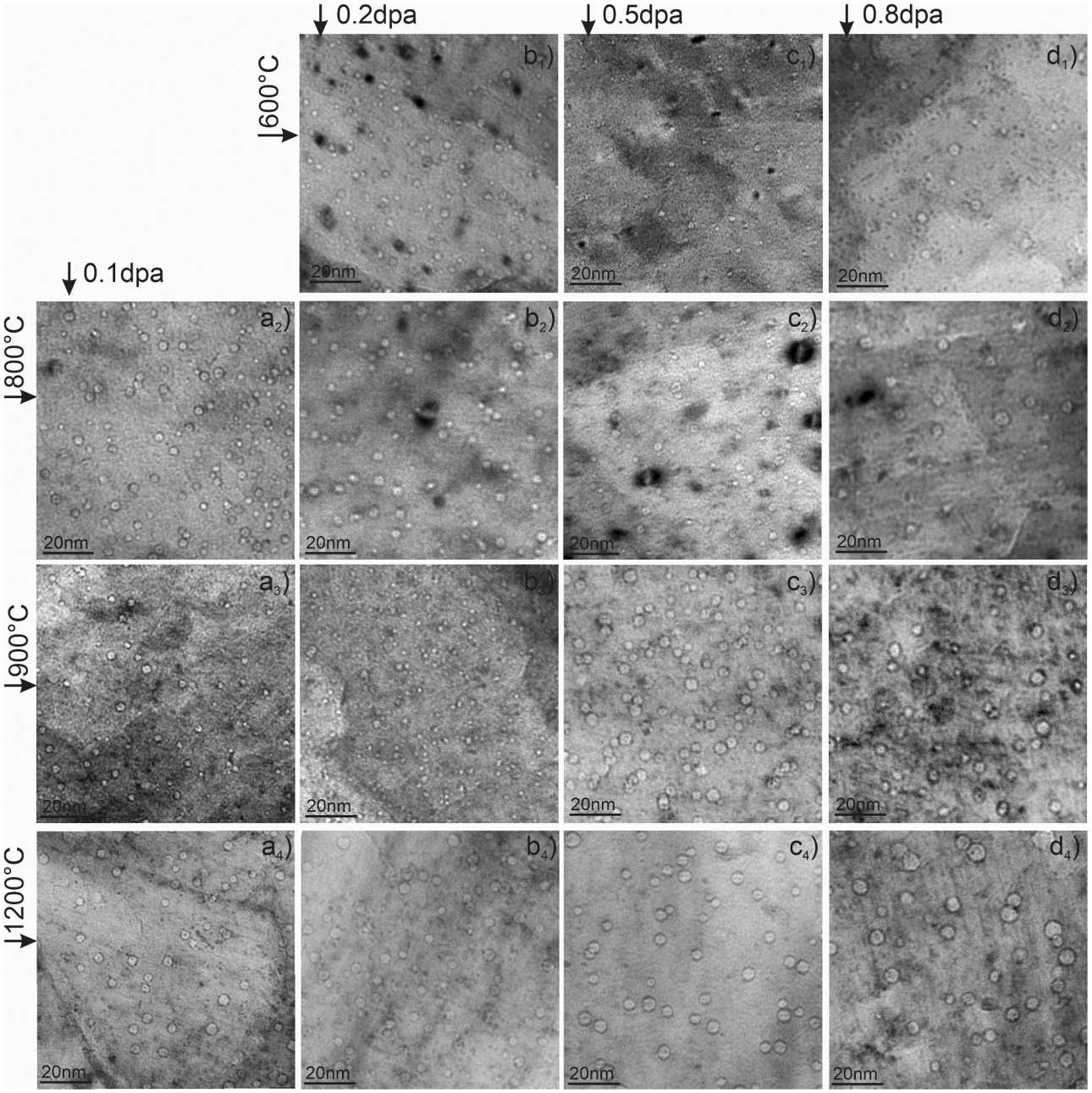

Fig. 2. BF TEM images showing voids in W irradiated 600°C (b_1-d_1), 800°C (a_2-d_2), 900°C (a_3-d_3) and 1200°C (a_4-d_4) at different doses, as marked in the images.

weak to be detectable at all defects. However, at higher damage doses, the void number density is lower than that of the clouds, since Re-segregation was also observed around the loops.

3.3. Inhomogeneities in the defect distribution

The voids are usually homogeneously distributed in the W, but the structural defects such as grain boundaries influence their formation, leading to local deviations from the average distribution. The formation of void denuded zone and void peak zone in the vicinity of grain boundaries was demonstrated in several studies [17–19]. Looking at the Re distribution at the grain boundaries, it could be concluded that the 20–25 nm thick layer around the grain or sub-grain boundaries is also free of Re clouds, indicating the absence of voids or dislocation loops. That is well visible considering Re and Os map shown in Figure 6a_1 or Figure 6c_1,c_2. This is quite evident, as Re- or Os- diffusion is strongly associated with the diffusion of vacancies or interstitials, which recombine at structural defects [20].

The study shows that the thickness of a defect denuded zone around the grain boundaries of is not the same in all cases. Fig. 7c shows a grain boundary with a Re cloud denuded zone of about 25 nm, as marked by the white line, on one side of the boundary and almost no denuded zone on the other side of the same boundary. The clouds are always associated with structural defects, either voids or dislocation loops, as has been shown in numerous publications [17,18]. The most likely reason for the absence of a denuded zone on one side is movement of the boundary under irradiation. It was demonstrated that besides voids and loops, neutron irradiation-induced recrystallization is also essential factor affecting mechanical properties of W [21]. Especially is this effect is strong at temperature >1000°C. The differences in the crystallographic grain orientation and the possibly associated different diffusion of vacancies or interstitials cannot serve as an explanation for this effect, since grain (2) shows the missing denudation zone at all boundaries.

It was also found that the defects in neighboring grains, despite

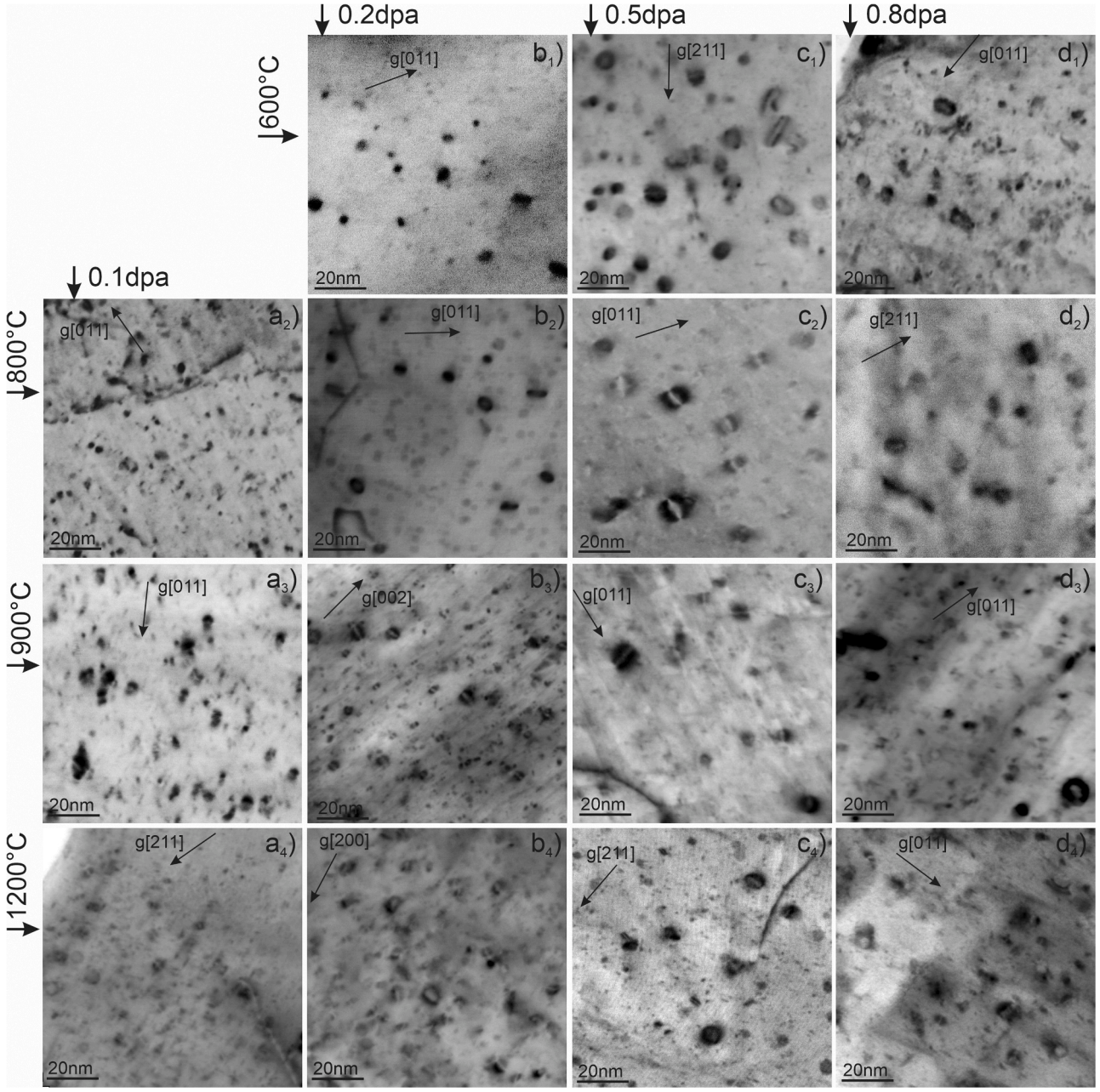

Fig. 3. DF TEM images with inverted contrast showing dislocation loops in W irradiated 600°C (b_1-d_1), 800°C (a_2-d_2), 900°C (a_3-d_3) and 1200°C (a_4-d_4) at different doses, as it marked in the images. The arrows in the images indicate the directions of the corresponding Burges vectors.

showing no noticeable differences, exhibit significantly different sizes and number densities. Fig. 8 demonstrates the distribution of Re clouds inside several grains in the sample irradiated to 0.5 dpa at 1200°C. The total investigated area that includes several grains has a horizontal field of view of 1125 nm (Fig. 8a). The two sections in parts (b) and (c) illustrate the areas within the white squares in the part (a) with higher magnification. The Re clouds inside the grain number (3) in part (b) have a three times lower number density and 30–40 % larger size than the clouds in the grains marked with (1) and (2) (Fig. 8b). The reason for such deviation remains unclear. The detailed TEM analysis does not show any recognizable amounts of impurities in the grain or other special features that could be the reason for such differences. We suggest that these most likely are impurities at a concentration below the EDS detection limit, which is in the range of ~0.1 at.%. This observation demonstrates that the defect formation in W can be significantly influenced by non-essential factors.

The elemental mapping can also be used to visualize defects that are not readily visible in the TEM. In the upper grain in Fig. 8a, two sub-grain boundaries and numerous line dislocations are visible. Looking at the area with linear dislocations, it can be recognized that the number density of clouds in the adjacent area is reduced. Presumably, the line dislocations have a similar effect on the defect formation as grain boundaries. For this reason, the formation of defects in highly deformed W could be significantly reduced, as a higher density of dislocations and grain boundaries serves as a sink for the vacancies and interstitial atoms [20]. It should be mentioned that these experimental observations are not due to the sample preparation in FIB.

4. Discussion

The analyzed material consists of elongated grains with a length of up to 3 μm and a width of up to 1 μm (Fig. 1a). Irradiation at 600°C with

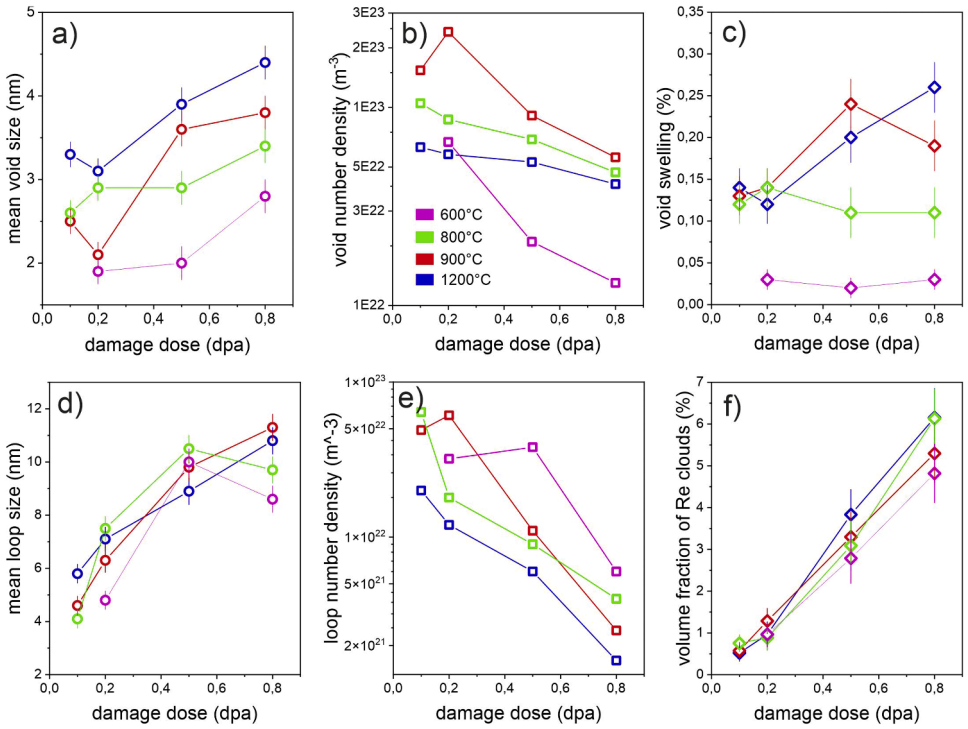

Fig. 4. The diagrams show the dose depended evolution of size (a,d) and number density (b,e) of the voids and dislocation loops irradiated at different temperatures, as well as void swelling (c) and volume fraction of Re-clouds. The data of the different irradiation temperatures are shown in different colors.

Table 2
Quantitative data of voids, loops and Re-clouds.

		Voids			loops		Re clouds
T_{irr}	damage dose (dpa)	average size (nm)	number density ($\times 10^{22}$ m^{-3})	void swelling (%)	average size (nm)	number density ($\times 10^{22}$ m^{-3})	number density ($\times 10^{22}$ m^{-3})
600°C	0.2	1.9	6.7	0.03 %	4.8	3.2	3.6
	0.5	2.0	2.1	0.02 %	10.0	3.8	7.3
	0.8	2.8	1.3	0.03 %	8.6	5.5	9.2
800°C	0.1	2.6	10.5	0.12 %	3.6	6.4	4.2
	0.2	2.9	8.7	0.14 %	7.2	1.8	3.3
	0.5	2.9	6.9	0.11 %	10.5	0.9	5.9
	0.8	3.4	4.7	0.11 %	9.7	0.3	8.8
900°C	0.1	2.5	15.3	0.13 %	4.6	5.0	3.2
	0.2	2.1	24.2	0.14 %	4.2	6.0	4.8
	0.5	3.6	9.1	0.24 %	8.5	1.1	6.3
	0.8	3.8	5.6	0.18 %	11.3	0.25	7.6
1200°C	0.1	3.3	6.3	0.14 %	5.8	2.0	2.9
	0.2	3.1	5.8	0.12 %	7.9	1.2	3.0
	0.5	3.9	5.3	0.20 %	8.9	0.6	5.5
	0.8	4.4	4.1	0.22 %	10.8	0.15	6.8

0.1 dpa does not result in significant grain coarsening, meaning the microstructure shown in Fig. 1a can be regarded as being in its original state. The materials irradiated at 800°C with 0.8 dpa and 900°C with 0.8 dpa does not show any noticeable grain coarsening. However, a significant increase in grain size was observed at 1200°C irradiation temperature. The grains after irradiation to 0.8 dpa - the maximum dose in the study - have an increase in grain size of ~25 %. (Fig. 1c).

Recently published work has shown that the recrystallisation processes under neutron irradiation in pure W start at 850°C and lead to a fivefold increase in grain size at 1100°C [21]. In our study, however, neutron irradiation caused only a slight (25 %) increase of the grain size at 1200°C-0.8 dpa. The reason for these differences could be that in our study a very limited area of approx. ~40 μm^2 (FIB lamella) was available for the examination of grains. Recrystallisation on neutron irradiated W has typically been studied using the optical microscopy or EBSD method, which allows the imaging of areas of several hundred micrometers with thousands of grains [21,22]. The second reason that methods diffraction contrast in TEM is more sensitive to the grain's orientation than EBSD or light microscopy. In the TEM, the grains are clearly visible due to the diffraction contrast, even if they have an orientation deviation of less than 0.3°. In EBSD, however, the grains with a misorientation of less than 3° are imaged as a single grain. Our TEM studies, which we carried out with W irradiated at >1000°C, show no significant recrystallisation in pure W [17].

Since no thermocouples were used in the present irradiation experiment, it is useful to make a note on the accuracy of determination of the irradiation temperature. Application of SiC samples as monitors to "read" the irradiation temperature post-mortem is a very common method since it allows for cost-effective solution avoiding out-of-pile equipment which otherwise is needed to organize in-situ temperature measurement. Based on the currently available literature information, the evaluation of the irradiation temperature using SiC can be performed

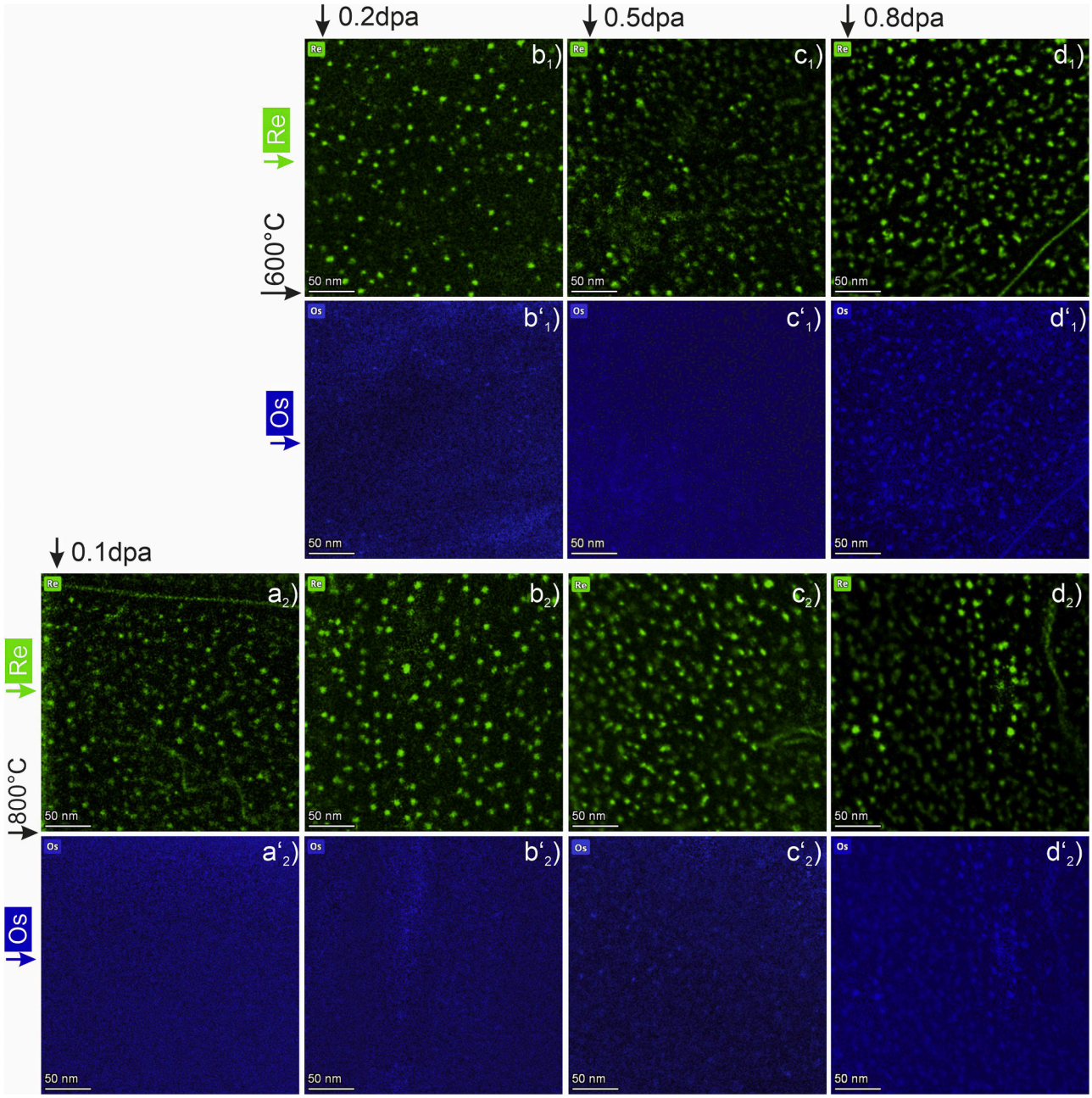

Fig. 5. STEM-EDX maps demonstrating the distribution of transmutation induced Re (green maps) and Os (blue maps) W irradiated at 600°C (b_1-d_1, b_1'-d_1') and 800°C (a_2-d_2, a_2'-d_2').

fairly accurately up to 600°C [23,24]. For higher irradiation temperatures, the accuracy of SiC monitors reduces due to the physical principles of the measurements involved [25]. An alternative way to evaluate the irradiation temperature is to perform 3D finite element model (FEM) calculations using MCNP output on the nuclear heat generation realized in the experimental assembly. For this method, it is essential that materials (material of the holder, or materials applied for thermal insulation) and fabrication technology involved are well known and the MCNP output is generated based on the actual positions of control rods and fuel burn-up throughout the cycle. In the present work, the irradiation temperature was confirmed by the post-irradiation 3D FEM calculations.

The study makes it possible to determine the evolution of the radiation induced defects as a function of the damage dose at different irradiation temperatures. The size and number density of both voids and dislocation loops exhibit a similar dependence on the damage. Their size increase with increasing damage (Fig. 4a,d), however, their number density decreases. The number density of the voids decreases by a factor of 2 to 3 as the damage dose increases to 0.8 dpa (Fig. 4b), while for loop it decreases by a factor of 20–50 (Fig. 4e). The reasons for this strong decrease is the Re segregation and precipitate formation on the loops [9], or/and the elastic loop-loop interaction that become more important as the loops size increase. The formation of precipitates that show a crystalline structure was only observed at 0.8 dpa damage and 900 and 1200°C irradiation temperatures. The occurrence of the defects is consistent with a formation diagram shown in refs. [9,26].

EDX mapping was used to measure size and number density of Re segregation sites. It was found that Re-rich clouds of –8 nm at lower damage doses and 10 nm - 13 nm at 0.8 dpa are formed on the voids and dislocation loops. The number density of Re clouds is higher than the

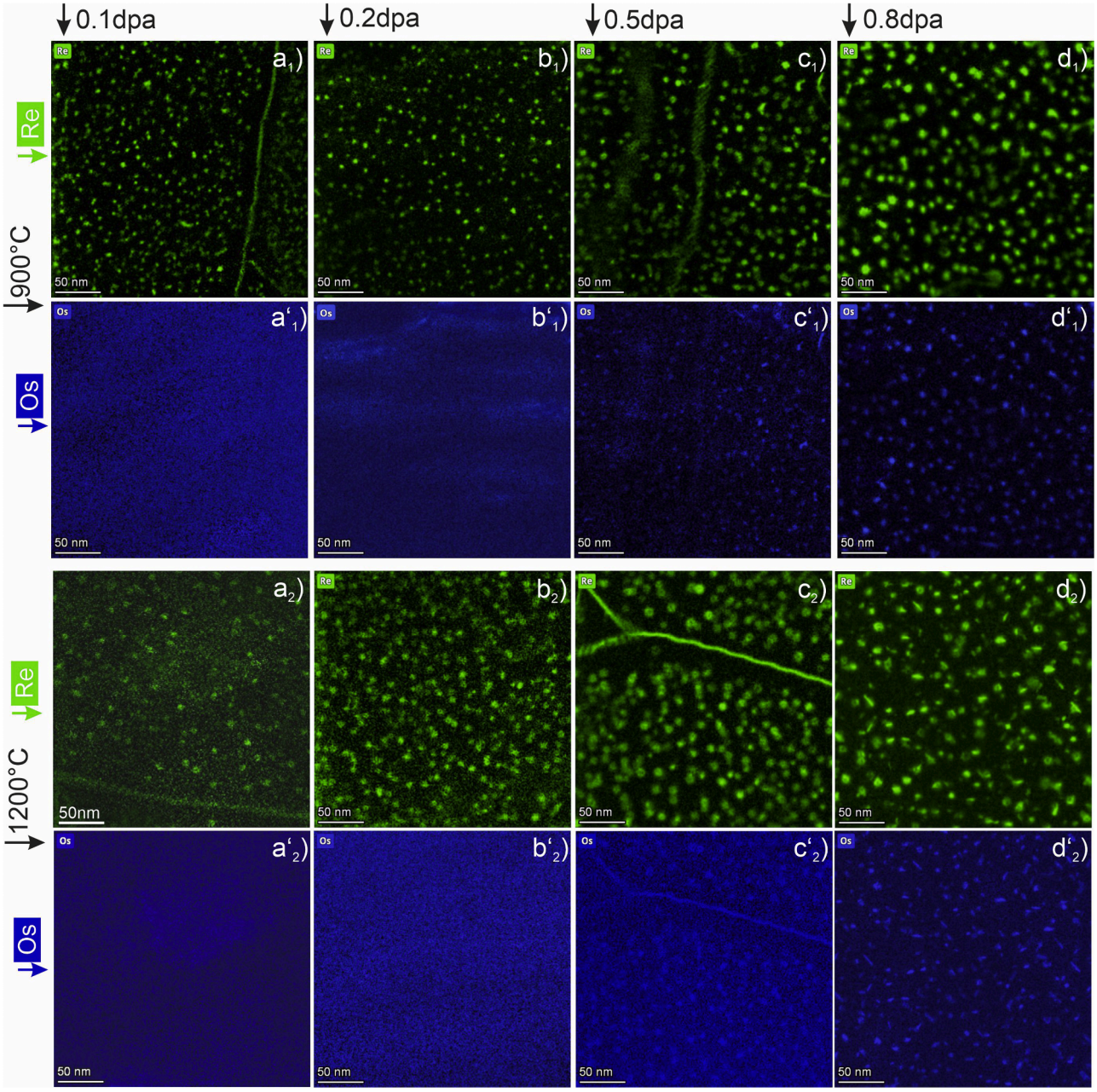

Fig. 6. STEM-EDX maps demonstrate distribution of transmutation induced Re (green maps) and Os (blue maps) W irradiated at 900°C (a_1-d_1, a_1'-d_1') and 1200°C (a_2-d_2, a_2'-d_2').

sum of the number densities of voids and loops. This is probably due to the fact that not all loops or voids are visible in TEM images, but the Re-segregation around these defects can be reliably identified in the EDX-mapping. The formation of nanosized precipitates could be proved only at 0.8 dpa at 900 and 1200°C. At lower temperatures the formation of precipitates could not be detected, but the EDX analysis shows the presence of a considerable number of Os-rich nuclei in the Re clouds, which can be regarded as precursors of precipitates. The inventory calculations show the formation of 1.9 % Re and 0.3 % Os at 0.8 dpa. HRTEM imaging shows that these precipitates exhibit a crystalline structure that differ from the matrix (Fig. 7). Since several atomic planes show a good similarity with the structure of χ-W(Re,Os)$_3$ phase, one can assume that the observed nanosized particles consist of this phase. However, due to their small size and overlap with the matrix, it is not possible to reliably determine their phase.

In the scientific literature, there are over a dozen studies on neutron-irradiated W that include TEM analysis of defects, that provide data on their size and number density [9,18,27–33]. The dose dependent defect parameters such as average size and number density including the data from this work are plotted in the diagrams shown in Fig. 9. The data from W irradiated in different reactors is also plotted with different symbols. W irradiation in HFIR reactors with a high fraction of neutrons with low energy ($E_n < 1$ MeV) leads to the production of up to 9 % Re per dpa. In contrast, irradiation in the Japanese experimental fast reactor JOYO leads to transmutation rates of only 1 % Re per dpa [34]. The differences in the transmutation rate are also reflected in the size and number density of the void and dislocation loops. Summarizing all these data, the following conclusions can be drawn about defect parameters in neutron irradiated W:

a) The defects size to a large extent does not depend on the radiation conditions. The size is limited in most cases to 5 nm for voids and to

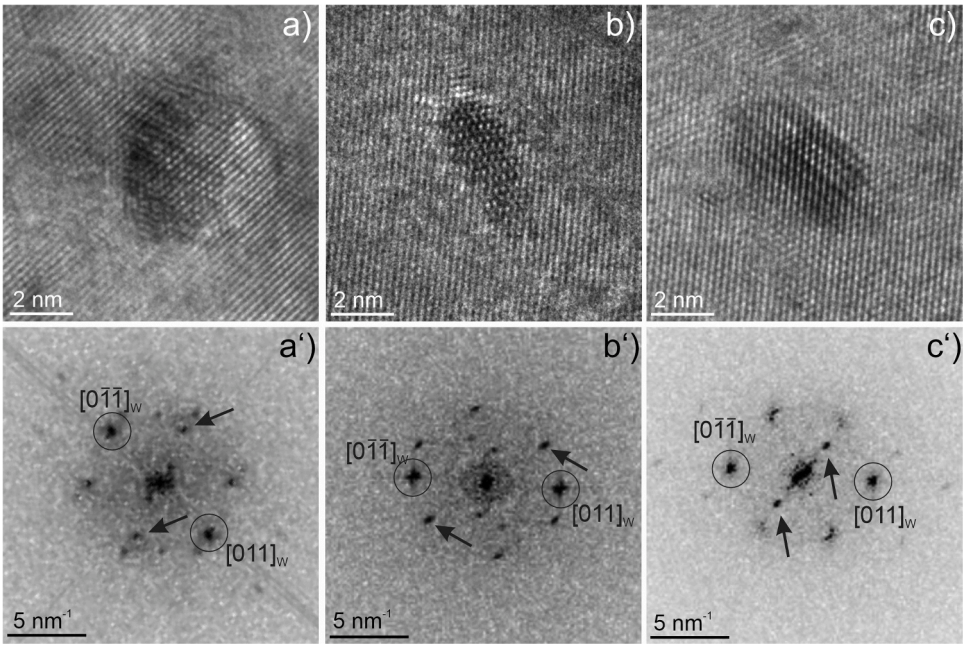

Fig. 7. HRTEM images of precipitates observed in W irradiated to 0.8 dpa at 1200°C (a) and at 900°C (b), (c). The images in (a'-c') show the corresponding Fourier transformation.

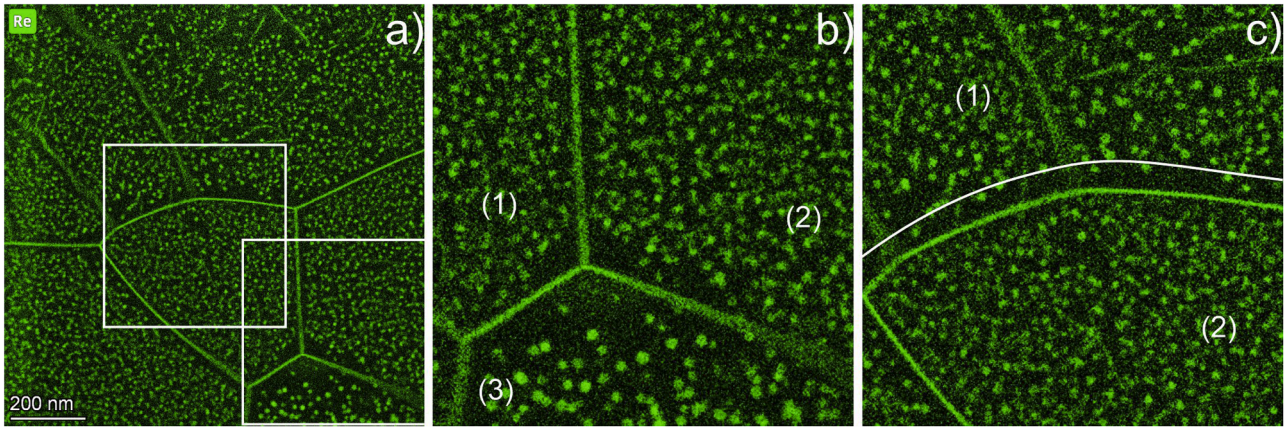

Fig. 8. Re distribution in several grains in the sample irradiated to 0.5 dpa at 1200°C demonstrating the inhomogeneities in the defect formations (a). Parts (b) and (c) show a detailed view of the sections marked by the white squares in part (a).

11 nm for loops. Voids with an average size below 2 nm were found in W irradiated in reactors with low transmutation rate. In these reactors, however, the loop size is markedly larger than in the HFIR reactor (Fig. 9a,c).

b) The number densities of the defects show a clear dependence on the reactor type and, herewith, on the transmutation rate and to a lesser extent on the irradiation conditions. The voids formed in W irradiated in HFIR tremendously have a lower number density and the loops higher number density than voids and loops formed reactors with lower transmutation rates (Fig. 9b,d).

The experimental data in Fig. 9 cover a total of ~50 experimental points obtained under various irradiation conditions. However, in contrast to our results, no clear dependence of the void and loop size or number density on the damage dose could be determined. The void size tends to increase at dose levels >1 dpa (Fig. 9a). It can also be seen that the loops formed in HFIR have a higher number density (red circles) than in BR2, JMTR or JOYO reactors (blue squares) (Fig. 9b,d). The assignment of this data to the references can be found in the supplementary Diagram 1 and the supplementary Table 1.

Our previous work has shown that the Re and Os play a significant role in the formation of dislocation loops [9]. Due to the radiation induced diffusion, Re and Os are segregated at structural defects. Starting from a certain Re and Os content, this leads to the formation of precipitates, which in turn influence the coarsening and evolution of defects. Since the difference in the transmutation rate in different reactor types can amount to a value of approx. 10, the reactor type has a decisive influence on the formation of defects. This should be considered when assessing the material for application in fusion reactors, as the transmutation rate there is an order of magnitude lower than in fusion reactors.

The reduction of the loop number density by one or more orders of magnitude at damage doses between 0.5 and 1 dpa also reflects the initial stages of precipitate formation (Fig. 9d). However, the limited amount of experimental data does not allow further conclusions. This scattering of experimental results can be explained by the fact that during irradiation such parameters as the cycle time, temperature stability, shielding, reactor type and other factors are different for various

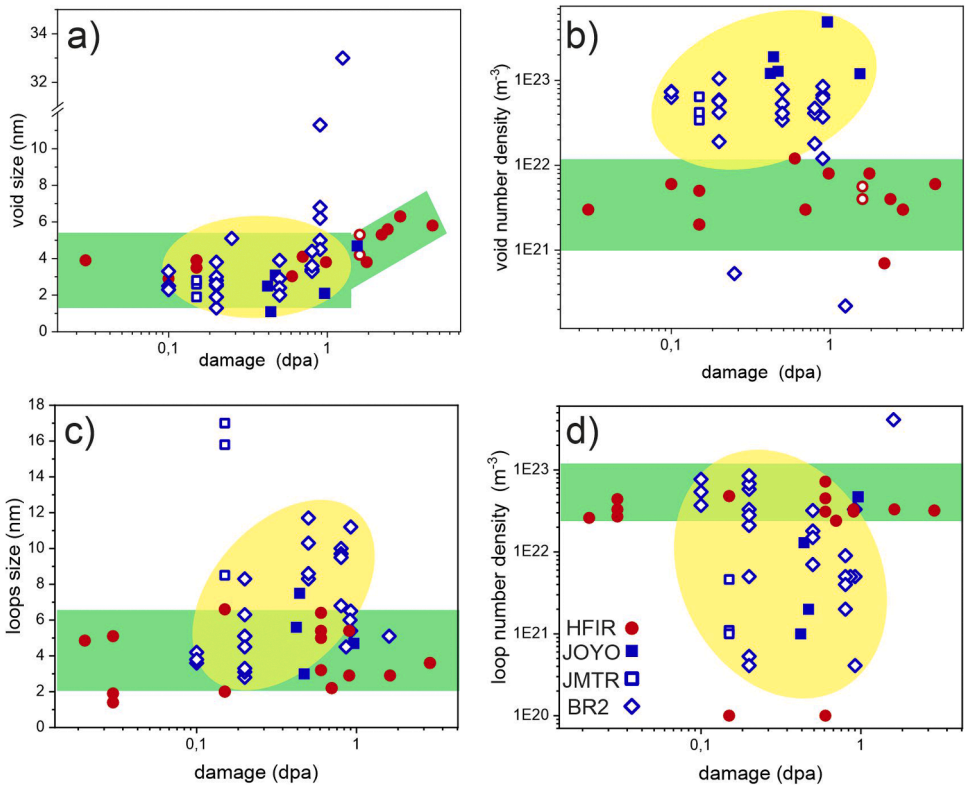

Fig. 9. The diagrams showing the size (a,c) and number density (b,d) of voids and dislocation loops formed in neutron irradiated W according to the literature [2,12,13,17–19,27,28,31,35–40]. The data points of W irradiation in reactors with high transmutation rates (>5 %Re/dpa, e.g., HFR/HFIR) are marked with red circles, whereas those with lower transmutation rates (JOYO, JMTR and BR2) are marked with blue squares. The green and yellow regions show the data ranges and expectations for these reactors.

irradiation experiments. It is impossible to keep the irradiation conditions stable and reproducible in different experiments. However, these factors could affect the formation of defects, and since the differences in the size of the voids or loops are in a narrow range, the effect of the damage dose is also not evident.

Our results that are summarized in Fig. 4 demonstrate clearly that voids and loops show a tendency to grow with damage doses, whereas their number density reduces. These results were obtained from W irradiated under very similar conditions, and, consequently, the effect of the damage dose stated in these samples is more reliable than comparing results from various irradiation experiments (Fig. 9).

The distribution of radiation induced defects could also be analyzed using Re elemental maps. Re-rich clouds that are formed around voids and dislocation loops even at the lowest damage doses provides more reliable information about the defect distribution than TEM imaging. The reason for this is that the Re distribution can be determined on a large scale regardless of grain orientation, whereas the conditions for high quality TEM imaging of voids and dislocation loops must be fulfilled locally, i.e. for individual grains. However, this analysis does not provide any information as to whether the defects are voids or dislocation loops.

The Re accumulates around the voids and dislocation loops and forms a 3–5 nm thick layer. This can be identified on elemental maps as Re enriched clusters of 8–13 nm size [18]. The clusters are well detectable even in W irradiated to 0.1 dpa at all irradiation temperatures (Fig. 5,5). Their number density largely corresponds to that of the voids (Table 2). At higher damage doses, it is much higher due to the detectable segregation around the loops and precipitates. The presence of Os on the defects was detected starting from 0.5 dpa damage, where its concentration achieves 0.2 %. The precipitates were detected at 0.8 dpa, where they are visible with elongated shape in the Os maps and in the HRTEM images (Fig. 7). Due to the size of a few nanometers, the phase of the precipitates could not be clearly identified. The number density of Re-rich clouds decreases with increasing irradiation temperature.

The Re-map in Fig. 8a shows several specific features that can help us to understand the factors that influence the formation of defects in W. In almost all investigated samples the defects are distributed very similarly inside different grains. However, there are some exceptions as shown for example in Fig. 8b. The size of the Re/Os clouds in grain (3) is larger and the number density significantly lower than in the neighboring grains (1) and (2). The reason for this unusual distribution is not clear and may be due to minor factors that cannot be detected with TEM. For example, it is possible that local differences in the concentration of some minor alloying elements far below the sensitivity of EDX analysis may have a significant influence on the formation and evolution of defects.

The second feature concerns the differences in the defect-denuded zone at the grain boundaries. According to previous experimental observations and the theory for the formation of defect-denuded layers at grain boundaries, these should typically form uniformly on both sides of a boundary [9,17,18,28]. However, in the example shown in Fig. 8c the denuded zone is absent in the grain (2), while in the adjacent grain (1) the defect denuded layer is ~26 nm thick. The denuded zone is also missing at the other boundaries of the grain (2). The cause of this deviation is not fully understood. It can be suggested that the different voids formation in these grains or the movement of the grain boundaries due to radiation-induced recrystallisation, as shown in ref. [21] could lead to formation of such structures. The fraction of areas with denuded zones is normally insignificant compared to the total volume, but for W which grain size is less than 1 μm it can reach a value that affects the mechanical properties of the irradiated W. In general, such inhomogeneities are expected to occur in regions where local conditions (presence of grain boundaries or dislocations) affect the diffusion of interstitials and voids [41].

It has been also shown that the presence of line dislocations can also influence the formation of defects and distribution of Re and Os. In the upper grain (left side) of the map, shown in Fig. 8a, several dislocation lines and sub-grain boundaries are visible based on Re segregation. In the area next to them the number density of radiation induced defects is remarkably lower than in other parts of the grain. The line dislocations serve as recombination sites for vacancies and interstitial defects, reducing their concentration in the neighboring region and causing Re accumulation at the dislocations. This results in a reduction in the number density of voids and loops, which is confirmed by the TEM analysis.

The radiation induced migration of Re and Os atoms leads consequently to the segregation on dislocation loops and voids [9]. The mechanism of association of solute atoms with vacancies and interstitials and their diffusion is considered the most appropriate to explain this effect [20,42]. The first principles calculations demonstrate that solutes such as Re or Os are strongly bound to interstitial and vacancies then W atoms. As a result, diffusion with these defects and recombination at the line dislocations, grain boundaries, voids and dislocation loops lead to their enrichment with solute atoms.

5. Conclusions

This study focusses on the microstructural examination of W irradiated at four temperatures 600°C, 800°C, 900°C and 1200°C to four damage doses 0.1 dpa, 0.2 dpa, 0.5 dpa and 0.8 dpa. This experimental matrix includes a total of 15 samples, the analysis of which provides important information on the defect evolution with increasing damage dose. The investigations show that the size of void and loop size tend to increase, while their number density decreases with the damage dose at all irradiation temperatures. Since previous studies showed no obvious dependence of size or number density on irradiation parameters, the results can contribute to the understanding of defect formation and development in W.

The analytical study demonstrates that transmutation induced Re and Os segregate around voids, loops and grain boundaries at all irradiation temperatures. Nanoscale Re/Os-rich precipitates were detected in material irradiated up to 0.8 dpa (~2.4 % at Re). At this damage dose the fraction of Re-rich clusters increases to 7–8 % of the total sample volume. In addition to other defects, these clusters affect the functionality of W components under neutron irradiation.

The analytical investigation of Re- and Os-segregation on defects shows a considerable local variation in defect morphology in closely spaced grains. This demonstrates that the formation of defects in W is strongly influenced by local minor factors, possibly such as variations in the local concentration of impurity elements in a concentration of <0.1 %, variations in dislocation density, structure of grain boundaries, etc.

CRediT authorship contribution statement

M. Klimenkov: Writing – original draft, Methodology, Conceptualization. **U. Jäntsch:** Validation, Investigation. **M. Rieth:** Supervision, Project administration, Methodology, Conceptualization. **H.C. Schneider:** Methodology. **D. Terentyev:** Validation, Methodology, Formal analysis. **W. Van Renterghem:** Validation, Investigation.

Declaration of competing interest

The authors declare that they have no known competing financial interests or personal relationships that could have appeared to influence the work reported in this paper.

Acknowledgements

This work has been carried out within the framework of the EUROfusion Consortium, funded by the European Union via the Euratom Research and Training Programme (Grant Agreement No 101052200 — EUROfusion). Views and opinions expressed are however those of the author(s) only and do not necessarily reflect those of the European Union or the European Commission. Neither the European Union nor the European Commission can be held responsible for them.

Supplementary materials

Supplementary material associated with this article can be found, in the online version, at doi:10.1016/j.jnucmat.2025.155673.

Data availability

Data will be made available on request.

References

[1] G. Pintsuk, G. Aiello, S.L. Dudarev, M. Gorley, J. Henry, M. Richou, M. Rieth, D. Terentyev, R. Vila, Materials for in-vessel components, Fusion Eng. Des. 174 (2022) 112994, https://doi.org/10.1016/j.fusengdes.2021.112994.
[2] D. Terentyev, C. Yin, A. Dubinko, C.C. Chang, J.H. You, Neutron irradiation hardening across ITER diverter tungsten armor, Int. J. Refract. Met. Hard Mater. (2020) 105437, https://doi.org/10.1016/j.ijrmhm.2020.105437.
[3] M. Rieth, R. Doerner, A. Hasegawa, Y. Ueda, M. Wirtz, Behavior of tungsten under irradiation and plasma interaction, J. Nucl. Mater. 519 (2019) 334–368, https://doi.org/10.1016/j.jnucmat.2019.03.035.
[4] S. Noce, G. Dose, D. Flammini, V. Imbriani, G. Mazzone, F. Moro, S. Roccella, F. Romanelli, R. Villari, E. Visca, J.-H. You, Nuclear analyses for the design of the ITER-like plasma facing components vertical targets of the DEMO divertor, Fusion Eng. Des. 155 (2020) 111730, https://doi.org/10.1016/j.fusengdes.2020.111730.
[5] E. Gaganidze, A. Chauhan, H.-C. Schneider, D. Terentyev, B. Rossaert, J. Aktaa, Effect of irradiation temperature on the fracture-mechanical behaviour of tungsten irradiated to 1 dpa, J. Nucl. Mater. 556 (2021) 153200, https://doi.org/10.1016/j.jnucmat.2021.153200.
[6] S. Nogami, D. Terentyev, A. Zinovev, C. Yin, M. Rieth, G. Pintsuk, A. Hasegawa, Neutron irradiation tolerance of potassium-doped and rhenium-alloyed tungsten, J. Nucl. Mater. 553 (2021) 153009, https://doi.org/10.1016/j.jnucmat.2021.153009.
[7] A. Durif, M. Richou, G. Kermouche, M. Lenci, J.-M. Bergheau, Impact of tungsten recrystallization on ITER-like components for lifetime estimation, Fusion Eng. Des. 138 (2019) 247–253, https://doi.org/10.1016/j.fusengdes.2018.11.003.
[8] X. Hu, Recent progress in experimental investigation of neutron irradiation response of tungsten, J. Nucl. Mater. 568 (2022) 153856, https://doi.org/10.1016/j.jnucmat.2022.153856.
[9] M. Klimenkov, U. Jäntsch, M. Rieth, H.C. Schneider, D. Terentyev, W. van Renterghem, Influence of transmutation-induced re/Os content on defect evolution in neutron-irradiated W, J. Nucl. Mater. 592 (2024) 154950, https://doi.org/10.1016/j.jnucmat.2024.154950.
[10] A. Hasegawa, T. Tanno, S. Nogami, M. Satou, Property change mechanism in tungsten under neutron irradiation in various reactors, J. Nucl. Mater. 417 (2011) 491–494, https://doi.org/10.1016/j.jnucmat.2010.12.114.
[11] T. Tanno, A. Hasegawa, J.C. He, M. Fujiwara, M. Satou, S. Nogami, K. Abe, T. Shishido, Effects of transmutation elements on the microstructural evolution and electrical resistivity of neutron-irradiated tungsten, J. Nucl. Mater. 386-388 (2009) 218–221, https://doi.org/10.1016/j.jnucmat.2008.12.091.
[12] M. Fukuda, N.Kiran Kumar, T. Koyanagi, L.M. Garrison, L.L. Snead, Y. Katoh, A. Hasegawa, Neutron energy spectrum influence on irradiation hardening and microstructural development of tungsten, J. Nucl. Mater. 479 (2016) 249–254, https://doi.org/10.1016/j.jnucmat.2016.06.051.
[13] A. Dubinko, D. Terentyev, C. Yin, W. van Renterghem, B. Rossaert, M. Rieth, E. E. Zhurkin, A. Zinovev, C.C. Chang, S. van Dyck, G. Bonny, Microstructure and hardening induced by neutron irradiation in single crystal, ITER specification and cold rolled tungsten, Int. J. Refract. Met. Hard Mater. 98 (2021) 105522, https://doi.org/10.1016/j.ijrmhm.2021.105522.
[14] B. Horváth, R. Schäublin, Y. Dai, Flash electropolishing of TEM lamellas of irradiated tungsten, Nucl. Instrum. Methods Phys. Res. B 449 (2019) 29–34, https://doi.org/10.1016/j.nimb.2019.04.047.
[15] C.T. Rueden, J. Schindelin, M.C. Hiner, B.E. DeZonia, A.E. Walter, E.T. Arena, K. W. Eliceiri, ImageJ2: ImageJ for the next generation of scientific image data, BMC. Bioinformatics. 18 (2017) 529, https://doi.org/10.1186/s12859-017-1934-z.
[16] P. Xiu, H. Bei, Y. Zhang, L. Wang, K.G. Field, STEM characterization of dislocation loops in irradiated FCC alloys, J. Nucl. Mater. 544 (2021) 152658, https://doi.org/10.1016/j.jnucmat.2020.152658.
[17] M. Klimenkov, M. Dürrschnabel, U. Jäntsch, P. Lied, M. Rieth, H.C. Schneider, D. Terentyev, W. van Renterghem, Microstructural analysis of W irradiated at different temperatures, J. Nucl. Mater. 572 (2022) 154018, https://doi.org/10.1016/j.jnucmat.2022.154018.
[18] M. Klimenkov, U. Jäntsch, M. Rieth, H.C. Schneider, D. Armstrong, J. Gibson, S. G. Roberts, Effect of neutron irradiation on the microstructure of tungsten, Nucl. Mater. Energy 9 (2016) 480–483, https://doi.org/10.1016/j.nme.2016.09.010.

[19] M. Dürrschnabel, M. Klimenkov, U. Jäntsch, M. Rieth, H.C. Schneider, D. Terentyev, New insights into microstructure of neutron-irradiated tungsten, Sci. Rep. 11 (2021) 7572, https://doi.org/10.1038/s41598-021-86746-6.
[20] J.S. Wróbel, D. Nguyen-Manh, K.J. Kurzydłowski, S.L. Dudarev, A first-principles model for anomalous segregation in dilute ternary tungsten-rhenium-vacancy alloys, J. Phys. Condens. Matter Instit. Phys. J. 29 (2017) 145403, https://doi.org/10.1088/1361-648X/aa5f37.
[21] H. Gietl, T. Koyanagi, X. Hu, M. Fukuda, A. Hasegawa, Y. Katoh, Neutron irradiation-enhanced grain growth in tungsten and tungsten alloys, J. Alloys. Compd. 901 (2022) 163419, https://doi.org/10.1016/j.jallcom.2021.163419.
[22] A. Alfonso, D.Juul Jensen, G.-N. Luo, W. Pantleon, Thermal stability of a highly-deformed warm-rolled tungsten plate in the temperature range 1100–1250°C, Fusion Eng. Des. 98-99 (2015) 1924–1928, https://doi.org/10.1016/j.fusengdes.2015.05.043.
[23] K.G. Field, J.L. McDuffee, J.W. Geringer, C.M. Petrie, Y. Katoh, Evaluation of the continuous dilatometer method of silicon carbide thermometry for passive irradiation temperature determination, Nucl. Instrum. Methods Phys. Res. B 445 (2019) 46–56, https://doi.org/10.1016/j.nimb.2019.02.022.
[24] A.A. Campbell, W.D. Porter, Y. Katoh, L.L. Snead, Method for analyzing passive silicon carbide thermometry with a continuous dilatometer to determine irradiation temperature, Nucl. Instrum. Methods Phys. Res. B 370 (2016) 49–58, https://doi.org/10.1016/j.nimb.2016.01.005.
[25] L.L. Snead, A.M. Williams, A.L. Qualls, Revisiting the use of SiC as a post irradiation temperature monitor, in: M.L. Grossbeck, T.R. Allen, R.G. Lott, A. S. Kumar (Eds.), Effects of Radiation on Materials: 21st International Symposium, 2004, pp. 623–633. ASTM International100 Barr Harbor Drive, PO Box C700, West Conshohocken, PA 19428-2959.
[26] J. Marian, C.S. Becquart, C. Domain, S.L. Dudarev, M.R. Gilbert, R.J. Kurtz, D. R. Mason, K. Nordlund, A.E. Sand, L.L. Snead, T. Suzudo, B.D. Wirth, Recent advances in modeling and simulation of the exposure and response of tungsten to fusion energy conditions, Nucl. Fusion 57 (2017) 92008, https://doi.org/10.1088/1741-4326/aa5e8d.
[27] T. Tanno, M. Fukuda, S. Nogami, A. Hasegawa, Microstructure development in Neutron irradiated tungsten alloys, Mater. Trans. 52 (2011) 1447–1451, https://doi.org/10.2320/matertrans.MBW201025.
[28] M. Fukuda, K. Yabuuchi, S. Nogami, A. Hasegawa, T. Tanaka, Microstructural development of tungsten and tungsten–rhenium alloys due to neutron irradiation in HFIR, J. Nucl. Mater. 455 (2014) 460–463, https://doi.org/10.1016/j.jnucmat.2014.08.002.
[29] A. Hasegawa, M. Fukuda, S. Nogami, K. Yabuuchi, Neutron irradiation effects on tungsten materials, Fusion Eng. Des. 89 (2014) 1568–1572, https://doi.org/10.1016/j.fusengdes.2014.04.035.
[30] X. Hu, C.M. Parish, K. Wang, T. Koyanagi, B.P. Eftink, Y. Katoh, Transmutation-induced precipitation in tungsten irradiated with a mixed energy neutron spectrum, Acta Mater. 165 (2019) 51–61, https://doi.org/10.1016/j.actamat.2018.11.032.
[31] T. Koyanagi, N.K. Kumar, T. Hwang, L.M. Garrison, X. Hu, L.L. Snead, Y. Katoh, Microstructural evolution of pure tungsten neutron irradiated with a mixed energy spectrum, J. Nucl. Mater. 490 (2017) 66–74, https://doi.org/10.1016/j.jnucmat.2017.04.010.
[32] Y. Katoh, L.L. Snead, L.M. Garrison, X. Hu, T. Koyanagi, C.M. Parish, P. D. Edmondson, M. Fukuda, T. Hwang, T. Tanaka, A. Hasegawa, Response of unalloyed tungsten to mixed spectrum neutrons, J. Nucl. Mater. 520 (2019) 193–207, https://doi.org/10.1016/j.jnucmat.2019.03.045.
[33] D. Papadakis, S. Dellis, V. Chatzikos, E. Manios, I.E. Stamatelatos, S. Messoloras, K. Mergia, Neutron irradiation effects in different tungsten microstructures, Phys. Scr. 96 (2021) 124041, https://doi.org/10.1088/1402-4896/ac1eb2.
[34] A. Hasegawa, M. Fukuda, K. Yabuuchi, S. Nogami, Neutron irradiation effects on the microstructural development of tungsten and tungsten alloys, J. Nucl. Mater. 471 (2016) 175–183, https://doi.org/10.1016/j.jnucmat.2015.10.047.
[35] T. Tanno, A. Hasegawa, M. Fujiwara, J.-C. He, S. Nogami, M. Satou, T. Shishido, K. Abe, Precipitation of solid transmutation elements in irradiated tungsten alloys, Mater. Trans. 49 (2008) 2259–2264, https://doi.org/10.2320/matertrans.MAW200821.
[36] M. Fukuda, T. Tanno, S. Nogami, A. Hasegawa, Effects of re content and fabrication process on microstructural changes and hardening in neutron irradiated tungsten, Mater. Trans. 53 (2012) 2145–2150, https://doi.org/10.2320/matertrans.MBW201110.
[37] J. He, G. Tang, A. Hasegawa, K. Abe, Microstructural development and irradiation hardening of W and W–(3–26) wt%re alloys after high-temperature neutron irradiation to 0.15 dpa, Nucl. Fusion 46 (2006) 877–883, https://doi.org/10.1088/0029-5515/46/11/001.
[38] A. Chauhan, Q. Yuan, D. Litvinov, E. Gaganidze, H.-C. Schneider, D. Terentyev, J. Aktaa, Effect of temperature on the neutron irradiation-induced cavities in tungsten, Philosophical Magazine 102 (2022) 1665–1683, https://doi.org/10.1080/14786435.2022.2079750.
[39] X. Hu, T. Koyanagi, M. Fukuda, N.K. Kumar, L.L. Snead, B.D. Wirth, Y. Katoh, Irradiation hardening of pure tungsten exposed to neutron irradiation, J. Nucl. Mater. 480 (2016) 235–243, https://doi.org/10.1016/j.jnucmat.2016.08.024.
[40] L.M. Garrison, Y. Katoh, N.K. Kumar, Mechanical properties of single-crystal tungsten irradiated in a mixed spectrum fission reactor, J. Nucl. Mater. 518 (2019) 208–225, https://doi.org/10.1016/j.jnucmat.2019.02.050.
[41] P.C. Millett, A. El-Azab, S. Rokkam, M. Tonks, D. Wolf, Phase-field simulation of irradiated metals, Comput. Mater. Sci. 50 (2011) 949–959, https://doi.org/10.1016/j.commatsci.2010.10.034.
[42] T. Suzudo, A. Hasegawa, Suppression of radiation-induced point defects by rhenium and osmium interstitials in tungsten, Sci. Rep. 6 (2016) 36738, https://doi.org/10.1038/srep36738.